Journal of the Physical Society of Japan
Vol. 76, No. 5, May, 2007, 054003

Statistical Mechanical Study of Code-Division Multiple-Access Multiuser Detectors —Analysis of Replica Symmetric and One-Step Replica Symmetry Breaking Solutions—

Mika YOSHIDA*, Tatsuya UEZU,
Toshiyuki TANAKA[1], and Masato OKADA[2]

Graduate School of Humanities and Sciences, Nara Women's University, Nara 630-8506
[1]*Graduate School of Informatics, Kyoto University, Kyoto 606-8501*
[2]*Graduate School of Frontier Sciences, The University of Tokyo, Kashiwa, Chiba 277-8561*

(Received January 29, 2007; accepted March 5, 2007; published May 10, 2007)

We study the problem of performance evaluation of code-division multiple-access (CDMA) multiuser detectors by means of statistical mechanics using the replica method. The replica symmetric solutions were analyzed previously. As is well known, the replica symmetric solution becomes unstable when the temperature (magnitude of noise) is lowered. In this paper, we investigate both the behavior and the stability of the replica symmetric solutions in the low temperature region. We find that the solutions have complicated bifurcation structures in the low temperature region where the solutions coexist. We also find that there are two types of replica symmetry breaking, Almeida–Thouless (AT)-instability and freezing. We obtain the one-step replica symmetry breaking solution in each case. Further, we compare the theoretical results with the results from the Monte-Carlo simulations. Consequently, we find that the theoretical results agree with the numerical simulations.

KEYWORDS: CDMA, performance evaluation, replica method, replica symmetry breaking, spin glasses, anti-hopfield model
DOI: 10.1143/JPSJ.76.054003

1. Introduction

The method for the performance evaluation of code-division multiple-access (CDMA) multiuser detectors in the large-system limit was established by Tanaka using the replica method.[1)] Since then, many studies have shown that the replica method is applicable in many cases, such as arbitrary input distribution,[2)] arbitrary additive channel noise,[3)] and MIMO (multi-input multi-output) channels.[4–6)]

Although the validity for the replica method in mathematics has not been proved yet, this method turns out to be very useful because it has been applied in many models and results have not contradicted any numerical simulations. In the replica analysis, first of all, solutions are derived under the assumption of replica symmetry. It is necessary to investigate the stability of replica symmetric (RS) solutions, and when stability breaks, the replica symmetry breaking solutions have to be considered. However, in previous studies of CDMA models, only the RS solutions have been considered.

We treat a model of the binary phase shift keying direct-sequence CDMA (BPSK-DS/CDMA) system. We consider additive white Gaussian channel noise and the marginal posterior mode (MPM) detector and evaluate its performance. The conditions for the breaking of replica symmetry in this system were established by Tanaka.[1)] When the posterior of the MPM detector is written in the form of canonical distribution, the Hamiltonian of this system is similar to that of a spin glass model with an external field and to that of the anti-Hopfield model in neural networks.[7,8)] In spin glass models, the anti-Hopfield model and others, RS solutions become unstable at low temperatures. In the CDMA models, the temperature parameter corresponds to the variance of channel noise. In this paper, we focus on low temperature regions since this is where the breaking of replica symmetry is expected. We investigate the behavior and Almeida–Thouless (AT)-stability, entropies, and the free energies of RS solutions in the low temperature regions. Appropriate solutions are AT-stable and have non-negative entropies. Further, when solutions coexist, the solution which has the minimum free energy should be identified. When the replica symmetry breaks, we investigate the behavior of one-step replica symmetry breaking (1RSB) solutions.[9)]

The results are as follows. When the temperature is lowered, the coexistence region of RS solutions appears. In this region, RS solutions have complicated bifurcation structures. As for the stability of RS solutions, there are two types of replica symmetry breaking: AT-instability RSB, and freezing RSB in which the entropy becomes 0. In both cases, 1RSB solutions are obtained. The results by Monte-Carlo simulations agree with the theoretical results, except where RS solutions coexist and thermodynamic transition temperature is as low as $T = 0.05$.

The paper is organized as follows: In §2, we explain the model. See ref. 1 for details. In §3, we describe the behavior of RS solutions, and in §4, we investigate the stability of the RS solution and derive the 1RSB solutions. In §5, we compare the theoretical results with the results by the Monte-Carlo simulations. Section 6 is devoted to summary and discussion.

2. The Model

Now we consider the N-user CDMA channel. The information bit of user i is denoted by η_i, which takes a ± 1 value. The spreading sequence of user i is $\{\xi_i^\mu; \mu = 1, \ldots, p\}$, and $\xi_i^\mu = \pm 1$. We assume that η_i and ξ_i^μ are independently generated from identical unbiased distributions. Further, we assume that the channel noise is additive white Gaussian noise $\{n^\mu; \mu = 1, \ldots, p\}$ with a

*E-mail: mika@ki-rin.phys.nara-wu.ac.jp

mean of 0 and a variance of σ_0^2. Then, the received signal is expressed as follows:

$$y^\mu = \frac{1}{\sqrt{N}} \sum_{i=1}^{N} \xi_i^\mu \eta_i + n^\mu \quad (\mu = 1, \ldots, p). \tag{1}$$

For later use, we define $\boldsymbol{y} \equiv (y^1, \ldots, y^p)^{\mathrm{T}}$, $\boldsymbol{\eta} \equiv (\eta_1, \ldots, \eta_N)^{\mathrm{T}}$, $\boldsymbol{n} \equiv (n^1, \ldots, n^p)^{\mathrm{T}}$, and $(\xi)_{\mu i} \equiv \xi_i^\mu$, $\mu = 1, \ldots, p$; $i = 1, \ldots, N$, where T denotes the transpose. Then, the relation (1) is expressed as

$$\boldsymbol{y} = \frac{1}{\sqrt{N}} \xi \boldsymbol{\eta} + \boldsymbol{n}.$$

Since the channel noise is Gaussian, the conditional distribution of the received signals $\boldsymbol{y}$, conditioned on the information bits $\boldsymbol{\eta}$ given the spreading sequences ξ, is expressed as follows:

$$p(\boldsymbol{y} \mid \boldsymbol{\eta}, \xi) = \frac{1}{\sqrt{2\pi\sigma_0^2}} \exp\left(-\frac{1}{2\sigma_0^2} \left\| \boldsymbol{y} - \frac{1}{\sqrt{N}} \xi \boldsymbol{\eta} \right\|^2 \right), \tag{2}$$

where σ_0^2 is the variance of the true Gaussian distribution and $\| \cdot \|$ denotes the Euclidean norm.

CDMA multiuser detectors decode the true information bit $\boldsymbol{\eta}$ from the received signal $\boldsymbol{y}$ and the spreading sequence ξ.[10] Let us denote the estimated value of $\boldsymbol{\eta}$ by $\boldsymbol{s} \equiv (s_1, \ldots, s_N)^{\mathrm{T}}$ where $s_i = \pm 1$. Then, the conditional distribution of the received signal $\boldsymbol{y}$, conditioned on information bit $\boldsymbol{s}$ given the spreading sequences ξ, is expressed as

$$p(\boldsymbol{y} \mid \boldsymbol{s}, \xi) = \frac{1}{\sqrt{2\pi\sigma^2}} \exp\left(-\frac{1}{2\sigma^2} \left\| \boldsymbol{y} - \frac{1}{\sqrt{N}} \xi \boldsymbol{s} \right\|^2 \right), \tag{3}$$

where σ^2 is the variance of the posterior Gaussian distribution, and, in general, differs from the variance σ_0^2 of the true Gaussian distribution. To estimate $\boldsymbol{s}$, it is necessary to know the posterior distribution $p(\boldsymbol{s} \mid \boldsymbol{y}, \xi)$ that is the conditional distribution of $\boldsymbol{s}$ conditioned on $\boldsymbol{y}$ given ξ. Assuming uniform prior distribution, by the Bayesian formula,[11–13] the posterior distribution is given as follows:

$$p(\boldsymbol{s} \mid \boldsymbol{y}, \xi) = \big(Z(\boldsymbol{y}, \xi)\big)^{-1} \exp\left(-\frac{1}{2\sigma^2} \| \boldsymbol{y} - N^{-1/2} \xi \boldsymbol{s} \|^2 \right), \tag{4}$$

$$Z(\boldsymbol{y}, \xi) = \sum_{\boldsymbol{s}} \exp\left(-\frac{1}{2\sigma^2} \| \boldsymbol{y} - N^{-1/2} \xi \boldsymbol{s} \|^2 \right). \tag{5}$$

Here we define temperature parameters as $T_0 = \beta_0^{-1} = \sigma_0^2$ and $T = \beta^{-1} = \sigma^2$, then the above posterior distribution can be rewritten as a canonical distribution with a Hamiltonian $H(\boldsymbol{s})$ as follows:

$$p(\boldsymbol{s} \mid \boldsymbol{y}, \xi) = \big(Z(\beta)\big)^{-1} \exp(-\beta H(\boldsymbol{s})), \tag{6}$$

$$Z(\beta) = \sum_{\boldsymbol{s}} \exp(-\beta H(\boldsymbol{s})), \tag{7}$$

$$H(\boldsymbol{s}) = \frac{1}{2} \sum_{ij} J_{ij} s_i s_j - \sum_i h_i^0 s_i, \tag{8}$$

$$J_{ij} = \frac{1}{N} \sum_{\mu=1}^{p} \xi_i^\mu \xi_j^\mu, \quad h_i^0 = \frac{1}{\sqrt{N}} \sum_{\mu=1}^{p} \xi_i^\mu y^\mu. \tag{9}$$

We find that the Hamiltonian $H(\boldsymbol{s})$ is similar to that of spin glass models with an external field and the anti-Hopfield model.[7,8]

$Z(\beta)$ is the partition function, and the free energy of this system F is given by $F = -1/\beta \log Z(\beta)$. We assume self-averaging in the large system limit $N, p \to \infty$, in which $\alpha \equiv p/N$ is fixed to a positive constant. Then the free energy per user becomes equal to the averaged free energy per user over the information symbols, the spreading sequences and the noise. Therefore, in the following, we evaluate the averaged free energy per user f. Then, f is expressed as

$$f = -\lim_{N \to \infty} \frac{1}{\beta N} \big[\log Z(\beta) \big],$$

where $[\cdot]$ denotes the average over information symbols, spreading sequences and noise. To evaluate $[\log Z(\beta)]$, we use the replica method. In the replica method, we use an identity

$$\big[\log Z(\beta) \big] = \lim_{n \to 0} \frac{\big[Z(\beta)^n \big] - 1}{n}.$$

We calculate $[Z(\beta)^n]$ for an integer n. Then taking the $n \to 0$ limit, we obtain $[\log Z(\beta)]$. Introducing n replicated random variables $\boldsymbol{s}^a = (s_1^a, \ldots, s_N^a)^{\mathrm{T}}$, $a = 1, \ldots, n$, $Z(\beta)^n$ is expressed as follows:

$$Z(\beta)^n = \prod_{a=1}^{n} \sum_{\boldsymbol{s}^a} \exp\left(-\frac{1}{2\sigma^2} \| \boldsymbol{y} - N^{-1/2} \xi \boldsymbol{s}^a \|^2 \right).$$

The macroscopic parameters R^a $(a = 1, \ldots, n)$ and q^{ab} $(a < b)$ are defined as follows:

$$R^a = \frac{1}{N} \boldsymbol{\eta}^T \langle \boldsymbol{s}^a \rangle, \quad q^{ab} = \frac{1}{N} \langle \boldsymbol{s}^a \rangle^T \langle \boldsymbol{s}^b \rangle. \tag{10}$$

Here, $\langle \cdot \rangle$ denotes the average over the posterior distribution. Further, we introduce $\hat{R}^a$ $(a = 1, \ldots, n)$ and $\hat{q}^{ab}$ $(a < b)$, which are the conjugate parameters of R^a and q^{ab}, respectively.

Under the replica symmetry ansatz $R^a = R$, $q^{ab} = q$, $\hat{R}^a = \hat{R}$, and $\hat{q}^{ab} = \hat{q}$, the free energy f_{RS} of the RS solution is given as

$$-\beta f_{\mathrm{RS}}(q, \hat{q}, R, \hat{R}, \beta, \beta_0, \alpha) = \alpha \left(-\frac{1}{2} \ln\big(1 + \beta(1 - q)\big) - \frac{\beta(1 + q - 2R + \beta_0^{-1})}{2\big(1 + \beta(1 - q)\big)} + \frac{1 + \beta_0}{2\beta_0} \beta \right) + \int Dz \ln\left(2\cosh(\sqrt{\hat{q}} z + \hat{R}) \right) - \frac{\hat{q}}{2}(1 - q) - R\hat{R}, \tag{11}$$

where $Dz \equiv \mathrm{d}z/\sqrt{2\pi} \exp(-z^2/2)$. From this, the saddle point equations (SPEs) are obtained as

$$R = \int Dz \tanh(\sqrt{\hat{q}}z + \hat{R}), \tag{12}$$

$$q = \int Dz \tanh^2(\sqrt{\hat{q}}z + \hat{R}), \tag{13}$$

$$\hat{R} = \frac{\alpha\beta}{1+\beta(1-q)}, \tag{14}$$

$$\hat{q} = \frac{\alpha\beta^2(q-2R+1+\beta_0^{-1})}{\big(1+\beta(1-q)\big)^2}. \tag{15}$$

The definition of R^a is given by eq. (10), that is, the overlap between the true information bit vector and its averaged estimate vector. If the true information bit vector and its averaged estimate vector agree, we obtain $R = 1$. The relationship between the overlap R and the bit-error rate P_b is $P_b = (1-R)/2$. So, we use the overlap R as an index to evaluate the performance of decoding.

3. Behavior of Solutions at Low Temperatures

At low temperatures, that is, in the case of small noise, we investigated the behavior of the RS solutions of SPEs.

It is known that RS solutions coexist at low temperatures. In Fig. 1, we display the α dependence of R at $T = T_0 = 0.05$. When the solutions coexist, we call three coexisting solutions branch 1, branch 2, and branch 3 as shown in Fig. 1.

The coexistence region of RS solutions at $T_0 = 0$ has been investigated in detail.[8] The spinodal line of this case in (α, T) space is shown in Fig. 2. We denote the boundary between branch 1 and branch 2 by $\alpha = \alpha_{1,2}(T)$, and the boundary between branch 2 and branch 3 by $\alpha = \alpha_{2,3}(T)$. $\alpha_{1,2}(T)$ is shown by a solid curve, and $\alpha_{2,3}(T)$ is shown by a dotted curve. The RS solutions coexist in the region enclosed by $\alpha_{1,2}(T)$ and $\alpha_{2,3}(T)$. $\alpha_{1,2}(T)$ is larger than $\alpha_{2,3}(T)$. As is clearly seen from Fig. 2, the region of α in which solutions coexist attains the maximum at $T = T_0 = 0$ and becomes gradually narrower as T becomes larger.

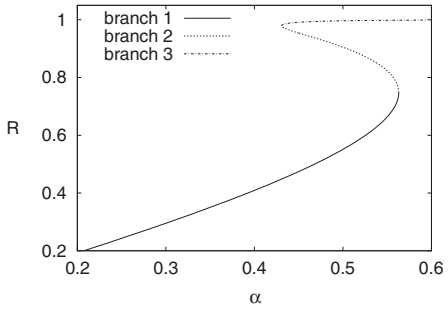

Fig. 1. Coexistence of solutions ($T = T_0 = 0.05$).

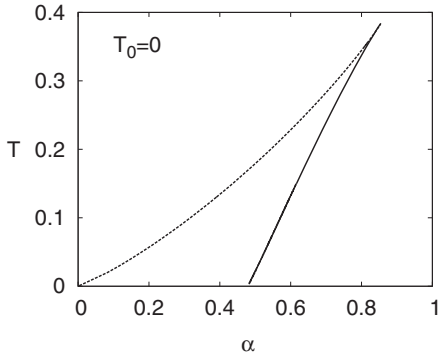

Fig. 2. Spinodal line at $T_0 = 0$. Solid curve: $\alpha_{1,2}(T)$, dotted curve: $\alpha_{2,3}(T)$.

Now, we investigate the case of $T_0 \neq 0$. To search for the coexistence region of RS solutions, we examined spinodal lines in (α, T) space with T_0 fixed (Fig. 3). From Fig. 3, we note that when T_0 is increased from 0, the maximum temperature T up to which the solutions coexist gradually decreases. At the same time, the region of coexistence of the solutions in the (α, T) space becomes smaller, and it

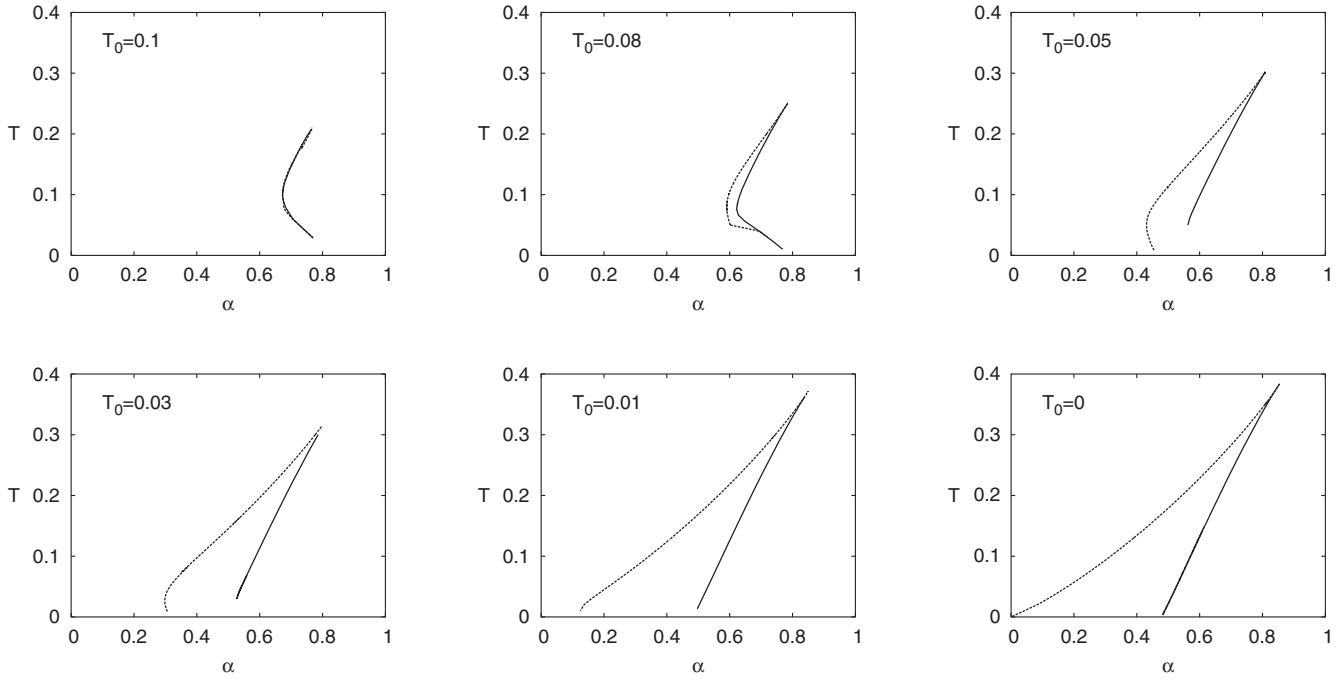

Fig. 3. Spinodal line. Solid curve: $\alpha_{1,2}(T)$, dotted curve: $\alpha_{2,3}(T)$.

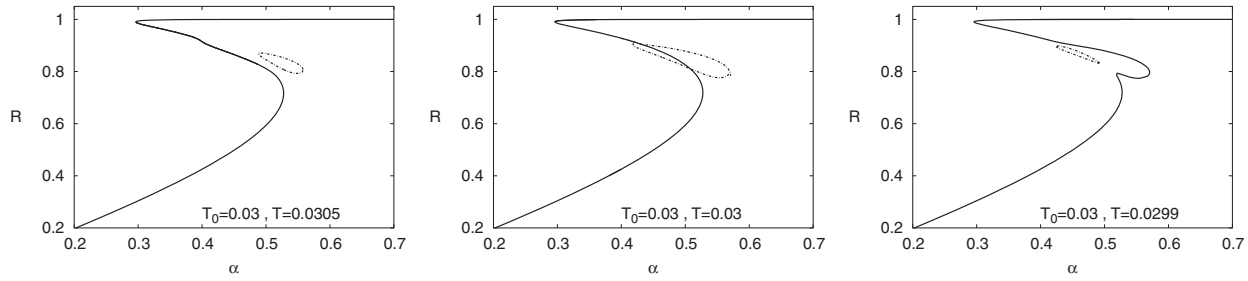

Fig. 4. α dependence of R at $T_0 = 0.03$. T is near T_0.

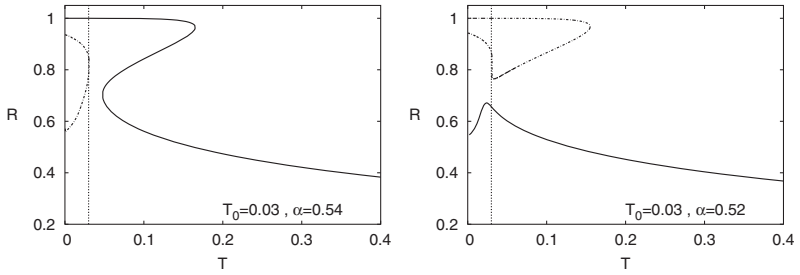

Fig. 5. T dependence of R at $T_0 = 0.03$. Vertical dotted line shows temperature $T = T_0$.

almost disappears at $T_0 = 0.1$. As for $\alpha = \alpha_{2,3}(T)$ (i.e., the boundary between branch 2 and branch 3), we note that it attains the minimum value in the vicinity of $T = T_0$. Thus, it seems that the minimum value of α, above which branch 3 appears, is attained at $T \simeq T_0$. On the other hand, as for $\alpha = \alpha_{1,2}(T)$, i.e., the boundary between branch 1 and branch 2, when $T_0 \neq 0$, as temperature T is decreased below T_0, we found that it is very difficult to obtain $\alpha_{1,2}(T)$ numerically. This is because the solution has a different structure from that in Fig. 1, and we can no longer define branch 1 and branch 2. We study these structures in detail in the following.

We examined the α dependence of R with $T_0 = 0.03$ fixed and taking T near T_0 (Fig. 4). We find the continuous sigmoidal-shaped solution in the left and center panels of Fig. 4, by which the spinodal lines in Fig. 3 were obtained. In the left and center panels of Fig. 4, we find a closed curve which differs from it. As we can see in the center and right panels of Fig. 4, these solutions collide at the vicinity of $T = T_0$, and are recombined to two separate solutions.

We also examine the T dependence of R with T_0 and α fixed. In Fig. 5, we display the T dependence of R at $T_0 = 0.03$, $\alpha = 0.54$ (left panel) and at $T_0 = 0.03$, $\alpha = 0.52$ (right panel). There are two separate solutions in the left panel of Fig. 5. One is a continuous sigmoidal-shaped solution. The other is a solution which exists only in the low temperature region of $T \leq T_0$. As noted from the results of the spinodal lines, the boundary value of α between branch 1 and branch 2 of the sigmoidal-shaped solution becomes smaller as temperature T is lowered. When the boundary reaches the vicinity of $T = T_0$, it connects to the other solution, and the recombination of the solutions takes place as in the right panel of Fig. 5.

Since branch 1 cannot be defined when the recombination takes place in the vicinity of $T = T_0$, a continuous spinodal line cannot be defined either.

4. Spinodal Lines, AT-Lines, Zero-Entropy Lines, and One-Step Replica Symmetry Breaking (1RSB) Solutions

In the previous section, we showed the behavior of the RS solutions at low temperatures. In this section, since at low temperatures the breaking of replica symmetry is observed in similar models such as spin glass models with similar Hamiltonians to the present model, we investigate the stability of the RS solutions and when it breaks, we derive 1RSB solutions.

Entropy s_{RS} is defined as the partial derivative of the free energy with respect to T:

$$s_{\mathrm{RS}} = -\frac{\partial}{\partial T} f_{\mathrm{RS}} = \frac{\hat{R}(1-q-2R)}{2} - \hat{q}(1-q) - \frac{\alpha}{2}\ln(1+\beta(1-q)) + \int Dz \ln\left(2\cosh(\sqrt{\hat{q}}z + \hat{R})\right).$$

The eigenvalue λ of the replicon mode in the RS solution is obtained as follows:[14)]

$$\lambda = 1 - \frac{\alpha\beta^2}{(1+\beta(1-q))^2}\int Dz\,\mathrm{sech}^4(\sqrt{\hat{q}}z + \hat{R}).$$

The zero-entropy lines and the AT-lines are defined as

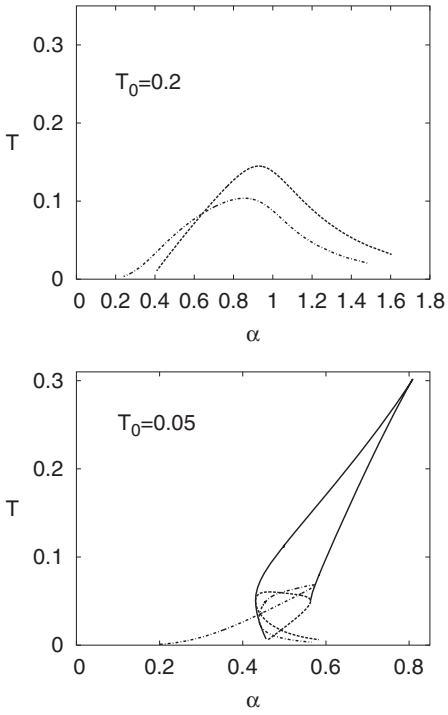

Fig. 6. Spinodal line (solid curve), AT-line (dashed curve) and zero-entropy line (dashed-dotted curve). Upper panel: $T_0 = 0.2$. Lower panel: $T_0 = 0.05$.

$s_{\rm RS} = 0$ and $\lambda = 0$, respectively.

In the upper panel of Fig. 6, we display the AT-line and zero-entropy line in the (α, T) space at $T_0 = 0.2$, where the RS solutions do not coexist. In the lower panel of Fig. 6, in addition to the spinodal line, we display the AT-lines and the zero-entropy lines for all branches at $T_0 = 0.05$, where the RS solutions coexist. The region below the AT-line and zero-entropy line corresponds to the AT-unstable region and the freezing region where the RS entropy becomes negative.

Now, let us examine the AT-lines and zero-entropy lines at $T_0 = 0.2$. In this case, only one branch exists, and the AT-line and zero-entropy line have one humped shape. Two lines intersect at $\alpha = \alpha_c^{(1)} \simeq 0.65$. Therefore, as T is decreased, the freezing takes place first for $\alpha < \alpha_c^{(1)}$, and the AT-instability takes place first for $\alpha > \alpha_c^{(1)}$. Thus, as in the case that there are no coexistent RS solutions in the (α, T) space, when the AT-line and the zero-entropy line intersect, we find that the stability of the RS solution breaks because of the freezing in one region of α. In the other region of α, the stability of the RS solution breaks because of the AT-instability.

Next, let us look at the AT-lines and zero-entropy lines at $T_0 = 0.05$. See the lower panel of Fig. 6. The AT-lines for the three branches are connected. The same is true for the zero-entropy lines. These lines fold back on $\alpha_{1,2}(T)$, and for α near $\alpha_{1,2}(T)$ inside the coexistence region, the lower lines and upper lines correspond to branch 1 and branch 2, respectively. The lines also fold back on $\alpha_{2,3}(T)$, and for α near $\alpha_{2,3}(T)$ inside the coexistence region, the lower lines and upper lines correspond to branch 3 and branch 2, respectively. At $T_0 = 0.05$, the AT line and zero-entropy line for branch 2 intersect at $\alpha = \alpha_c^{(2)} \simeq 0.49$. Therefore, inside the coexistent α region, as T is decreased, the freezing takes place first for all α region for branch 1 and $\alpha_c^{(2)} < \alpha$ for branch 2, and the AT-instability takes place first for all α for branch 3 and $\alpha_c^{(2)} > \alpha$ for branch 2.

The AT-stability and the value of entropy in each branch change depending on T_0. We do not go into details here but only mention one common feature independent of T_0. That is, when the AT-line turns around at $\alpha_{2,3}(T)$ and $\alpha_{1,2}(T)$, T is equal to T_0 (Nishimori-line). It was proved theoretically by Tanaka.[1)]

Thus, we find two different scenarios of replica symmetry breaking, the freezing and the AT-instability. When α and T_0 are given, neither scenario of the RSB occurs when T is high enough. As T is decreased, either the AT-instability or the freezing occurs depending on α and T_0. We call the case in which the AT-instability takes place first, case 1, and in which the freezing takes place first, case 2, when T is decreased. Now, let us derive the RSB solution in each case.

In case 1, under the one-step replica symmetry breaking ansatz, the free energy $f_{\rm 1RSB}$ and the SPEs are obtained as

$$
\begin{aligned}
&-\beta f_{\rm 1RSB}(q_1, \hat{q}_1, q_0, \hat{q}_0, R, \hat{R}, m, \beta, \beta_0, \alpha) \\
&= \alpha\left(-\frac{1}{2}\ln\bigl(1+\beta(1-q_1)\bigr) - \frac{1}{2m}\ln\left(\frac{\varphi}{1+\beta(1-q_1)}\right)\frac{\beta(1+q_0-2R+\beta_0^{-1})}{2\varphi} + \frac{\eta}{2}(1+\beta_0^{-1})\right) \\
&\quad - \frac{\hat{q}_1}{2} + \frac{1}{m}I + \frac{1-m}{2}\hat{q}_1 q_1 - \frac{m}{2}\hat{q}_0 q_0 - R\hat{R}, \qquad (16)
\end{aligned}
$$

$$
q_1 = \int Dz \frac{1}{K}\int Dt\, \Omega^m \tanh^2(\sqrt{\hat{q}_0}z + \sqrt{\hat{q}_1 - \hat{q}_0}t + \hat{R}), \qquad (17)
$$

$$
q_0 = \int Dz \left\{\frac{1}{K}\int Dt\, \Omega^m \tanh(\sqrt{\hat{q}_0}z + \sqrt{\hat{q}_1 - \hat{q}_0}t + \hat{R})\right\}^2, \qquad (18)
$$

$$
R = \int Dz \frac{1}{K}\int Dt\, \Omega^m \tanh(\sqrt{\hat{q}_0}z + \sqrt{\hat{q}_1 - \hat{q}_0}t + \hat{R}), \qquad (19)
$$

$$
\hat{q}_1 = \alpha\beta^2 \frac{q_1 - q_0}{(1+\beta(1-q_1))(1+\beta(1-q_1)+m\beta(q_1-q_0))} + \hat{q}_0, \qquad (20)
$$

$$\hat{q}_0 = \frac{\alpha\beta^2(1+\beta_0^{-1}+q_0-2R)}{(1+\beta(1-q_1)+m\beta(q_1-q_0))^2}, \tag{21}$$

$$\hat{R} = \frac{\alpha\beta}{1+\beta(1-q_1)+m\beta(q_1-q_0)}, \tag{22}$$

$$\frac{(\hat{q}_1-\hat{q}_0)\{1+\beta(1-q_1)+m\beta q_1\}}{2\beta} = \frac{\alpha}{2m}\ln\left(\frac{1+\beta(1-q_1)+m\beta(q_1-q_0)}{1+\beta(1-q_1)}\right) - \frac{1}{m}I + \int Dz\frac{1}{K}\int Dt\,\Omega^m \ln\Omega, \tag{23}$$

$$\varphi = 1+\beta(1-q_1)+m\beta(q_1-q_0),$$
$$I = \int Dz \ln K, \quad K = \int Dt\,\Omega^m, \quad \Omega = 2\cosh(\sqrt{\hat{q}_0}z + \sqrt{\hat{q}_1-\hat{q}_0}t + \hat{R}).$$

In case 2, we take the Krauth–Mézard limit $q_1 \to 1$ and $\hat{q}_1 \to \infty$ as in the case of the Ising perceptron.[15] Though this is an ansatz, from the numerical results shown below, we consider it valid. Then, the free energy of the 1RSB solution $f_{\rm 1RSB}$ is related to that of the RS solution $f_{\rm RS}$ as

$$f_{\rm 1RSB}(q_1=1,\hat{q}_1=\infty,q_0,\hat{q}_0,R,\hat{R},m,\beta,\beta_0,\alpha) = f_{\rm RS}(q_0,m^2\hat{q}_0,R,m\hat{R},m\beta,\beta_0,\alpha). \tag{24}$$

The SPEs are those for the RS solution plus the zero entropy condition, $s_{\rm RS}=0$. When the solutions of these equations are denoted as q_c, $\hat{q}_c$, R_c, $\hat{R}_c$, and β_c, then the 1RSB solution is expressed by

$$q_0 = q_c, \qquad \hat{q}_0 = m^{-2}\hat{q}_c, \qquad R = R_c, \qquad \hat{R} = m^{-1}\hat{R}_c, \qquad m = \frac{\beta_c}{\beta}.$$

Since $m \le 1$, the 1RSB solution is valid for $T \le T_c$.

Now, we investigate the behavior of solutions in (α, T) space with T_0 fixed. See Fig. 6. First, we investigate the case in which there is no region of coexistence of RS solutions. In this case, as temperature T is lowered, case 2 takes place in the region for $\alpha < \alpha_c^{(1)}$ and case 1 takes place for $\alpha > \alpha_c^{(1)}$. Here, $\alpha_c^{(1)}$ is the value of α where the AT-line and the zero-entropy line intersect. We examine the T dependence of R in both cases. In the left panel of Fig. 7, we display the T dependence of R at parameters where case 1 takes place. This figure corresponds to the parameters indicated by the vertical solid line in the left panel of Fig. 8. In the right panel of Fig. 7, we display the T dependence of R at the parameters where case 2 takes place. This figure corresponds to the parameters indicated by the vertical dotted line in the left panel of Fig. 8. In both $\alpha = 0.9$ (left panel) and $\alpha = 0.6$ (right panel) cases, we find R of the

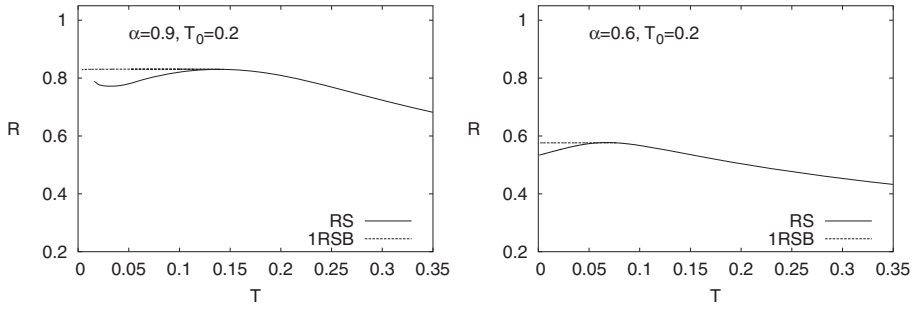

Fig. 7. T dependence of R. Solid curve: RS solution, dotted curve: 1RSB solution. Left panel: case 1, $\alpha = 0.9$ and $T_0 = 0.2$. Right panel: case 2, $\alpha = 0.6$ and $T_0 = 0.2$.

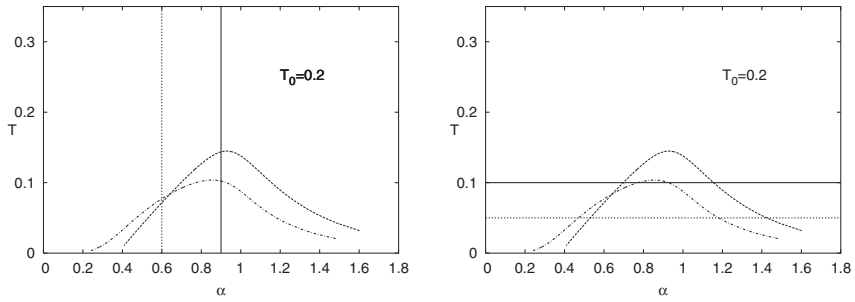

Fig. 8. AT-line (dashed curve) and zero-entropy line (dashed-dotted curve). $T_0 = 0.2$. Left panel: Vertical solid line is drawn at $\alpha = 0.9$ and vertical dotted line is at $\alpha = 0.6$. Right panel: Horizontal solid line is drawn at $T = 0.1$ and horizontal dotted line is at $T = 0.05$.

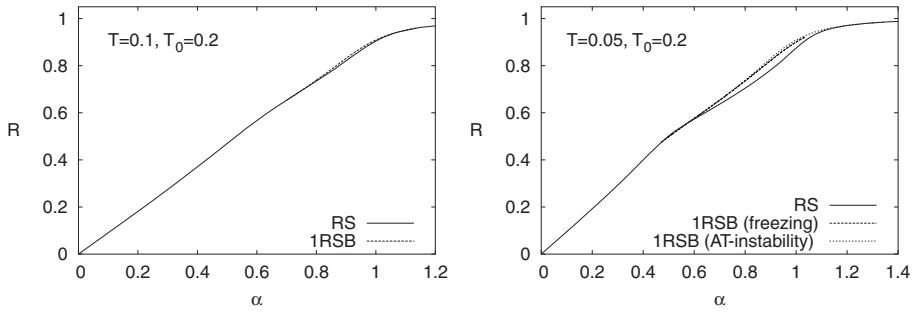

Fig. 9. α dependence of R. Solid curve: RS solution, dotted curve: 1RSB solution, left panel: $T = 0.1$ and $T_0 = 0.2$, right panel: $T = 0.05$ and $T_0 = 0.2$.

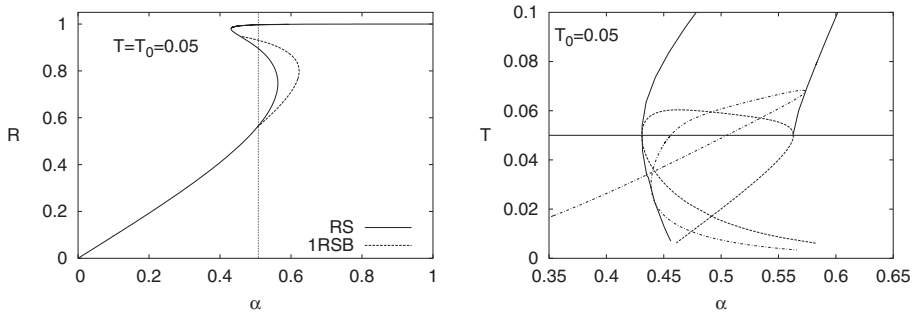

Fig. 10. Left panel: α dependence of R at the Nishimori temperature $T_0 = T = 0.05$. Solid curve: RS solution, dotted curve: 1RSB solution. Vertical dotted line indicates value α_{th}. Right panel: spinodal line (solid curve), AT-line (dotted curve) and zero-entropy line (dashed-dotted curve). Horizontal solid line indicates $T = 0.05$.

RS solution decreases at least initially as T is lowered from the temperature where the replica symmetry breaking takes place. We also find R of the 1RSB solution is larger than that of the RS solution.

Next, we show the results of the α dependence of R at $T_0 = 0.2$. In the left panel of Fig. 9, we display the result of the α dependence of R at $T = 0.1$ which is higher than the temperature where the AT-line and zero-entropy line intersect. This figure corresponds to the parameters indicated by the horizontal solid line in the right panel of Fig. 8. In the right panel of Fig. 9, we display the α dependence of R at $T = 0.05$, which is lower than the temperature of intersection. This figure corresponds to the parameters indicated by the horizontal dotted line in the right panel of Fig. 8. From the right panel of Fig. 8, we note that case 1 takes place at $T_0 = 0.2$ and $T = 0.1$. On the other hand, at $T_0 = 0.2$ and $T = 0.05$, case 2 takes place for $0.47 < \alpha < 1.18$ and case 1 does for $1.18 < \alpha < 1.42$. As seen from Fig. 9, in both cases the value of R for the RS solution approaches 1 as α becomes large. Furthermore, in both cases, though the value of R for the 1RSB solution is larger than that for the RS solution, the difference of R between the RS solution and 1RSB solution is very small.

Now, we investigate the case in which solutions coexist. As we discussed above, we found that case 1 takes place for branch 3 and case 2 takes place for branch 1 in this case. Furthermore, as seen from the right panel of Fig. 10, even at the Nishimori temperature $T = T_0$, case 2 takes place for branch 1. It is worth noting because it was proved by Nishimori that the RS solution is always stable at the Nishimori temperature.[16] So, we investigate the behavior of solutions at Nishimori temperature. In this paper, we show the results of $T = T_0 = 0.05$. We have obtained similar results at $T = T_0 = 0.01, 0.03$. As seen from the right panel of Fig. 10, we note that at the Nishimori temperature $T = T_0 = 0.05$, branch 1 is AT-stable in all α regions and has negative entropy in the large α region, branch 2 is AT-unstable in all α regions and has negative entropy in the large α region, and branch 3 is AT-stable and has positive entropy in all α regions. Thus, we do not consider branch 2 because of the AT-instability in all α regions. Let α_s be the value of α where the value of the entropy for branch 1 becomes 0. The region where the freezing 1RSB for branch 1 appears is $\alpha > \alpha_s$. In the left panel of Fig. 10, we display the α dependence of R at the Nishimori line $T = T_0 = 0.05$. The vertical dotted line in this figure indicates the value of α where the free energy f_1 for branch 1 of the RS solution becomes equal to the free energy f_3 for branch 3 of the RS solution. We denote this α value by α_{th}. For $\alpha < \alpha_{th}$, $f_1 < f_3$ and for $\alpha > \alpha_{th}$, $f_1 > f_3$. We compared α_s with α_{th} and found $\alpha_{th} < \alpha_s$ although α_{th} is very close to α_s. Therefore, we concluded that when α is increased from 0, the first order phase transition from the RS solution for branch 1 to that for branch 3 takes place at $\alpha = \alpha_{th}$. Both of the RS solutions are AT-stable and have positive entropies. We also obtained the same results at $T = T_0 = 0.01, 0.03$. Thus, in the case of $T = T_0$, when α is increased from 0, it is considered that the thermodynamic transition from the RS solution for branch 1 to that for branch 3 takes place just before the appearance of 1RSB solution due to the freezing, that is, the 1RSB solution for branch 1 is always metastable. Therefore, this result is consistent with the conclusion by Nishimori that the replica symmetry does not break on the Nishimori line.[16]

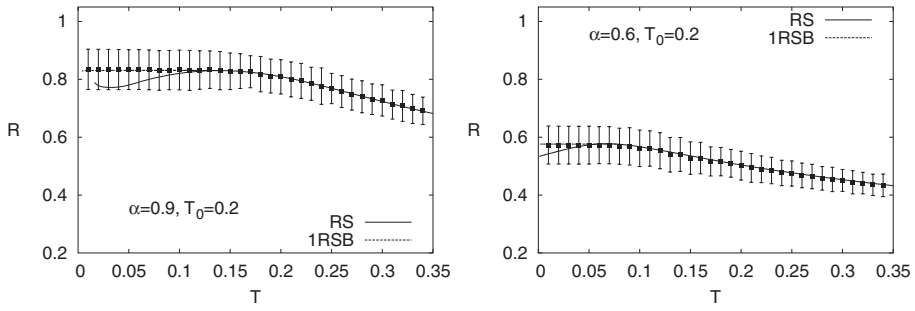

Fig. 11. T dependence of R. Solid curve: RS solution, dotted curve: 1RSB solution, $*$: simulation results with error bars. $N = 400$ and number of samples is 100. Left panel: case 1. $\alpha = 0.9$ and $T_0 = 0.2$. Right panel: case 2. $\alpha = 0.6$ and $T_0 = 0.2$.

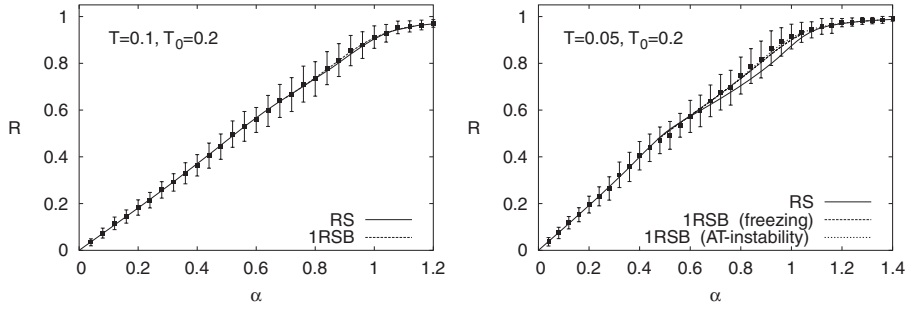

Fig. 12. α dependence of R. Solid curve: RS solution, dotted curve: 1RSB solution, $*$: simulation results with error bars. $N = 400$ and the number of samples is equal to 100. Left panel: Only case 1 takes place. $T = 0.1$ and $T_0 = 0.2$. Right panel: Both case 1 and case 2 take place. $T = 0.05$ and $T_0 = 0.2$.

5. Comparison between Theoretical Results and Numerical Simulations

In this section, we compare the theoretical results obtained in the previous sections and the results by Monte-Carlo simulations (MCS). Here, we briefly describe the method of simulation. We performed the MCS with an annealing procedure. We started the annealing procedure at $T = 1$ and then decreased to $T = 0.01$ in increments of $\Delta T = 0.01$. We confirmed that the results are the same when a different annealing schedule is adopted. For example we started at $\beta = 1$ and increased to $\beta = 200$ in increments of $\Delta\beta = 1$. We used several values for the system size. In this paper, we display the results for $N = 400$. We obtained almost the same results for the larger value of N. The information bit $\{\eta_i\}$, the spreading sequence $\{\xi_i^\mu\}$ and the initial condition $\{s_i\}$ of the estimate value of $\{\eta_i\}$ are independently generated from identical, unbiased distributions. The noise $\{n^\mu\}$ is generated from the Gaussian distribution. Generating different sets of $\{\xi_i^\mu\}$, $\{n^\mu\}$ and $\{s_i\}$ but fixing $\{\eta_i\}$, we took 100 samples.

First, we investigated the region where the RS solutions coexist. In Fig. 11, we display the simulation results of the T dependence of R, which correspond to the theoretical results of Fig. 7 at $T_0 = 0.2$ and $\alpha = 0.9$ (case 1, left panel) and $T_0 = 0.2$ and $\alpha = 0.6$ (case 2, right panel). As seen from Fig. 11, the simulation results agree with the theoretical results of the RS solutions in the high temperature region. On the other hand, in the low temperature region where the 1RSB solution exists, the values of R for both the RS and the 1RSB solutions lie within the error bars of simulations and in particular, the average value of the simulation agrees with the results of 1RSB solution very well.

Next, in Fig. 12, we display the simulation results of the α dependence of R, which correspond to the theoretical results of Fig. 9. At $T = 0.1$ and $T_0 = 0.2$ where only case 1 takes place (the left panel of Fig. 12), we cannot decide which of the RS or the 1RSB solutions is realized by the simulation because the 1RSB solution is very close to the RS solution. At $T = 0.05$, $T_0 = 0.2$ where both case 1 and case 2 take place (the right panel of Fig. 12), in the region where the 1RSB solutions appear, the values of R for both the RS and 1RSB solutions lie within the error bars of the simulations. In particular, the average value of the simulations agrees with the results of the 1RSB solutions very well.

Now, we investigate the case in which the RS solutions coexist. In particular, we focus on the situation where case 2 takes place for branch 1 on the Nishimori-temperature, $T = T_0$. From the theoretical analysis, it is expected that as α is increased from 0, a thermodynamic transition from the RS solution for branch 1 to that for branch 3 takes place just before the appearance of 1RSB solution due to the freezing. In Fig. 13, we display the simulation results of α dependence of R at the Nishimori temperature $T = T_0 = 0.05$, which corresponds to the theoretical result in the left panel of Fig. 10. The simulation results agree with the RS solution both for $\alpha < \alpha_s$ and for the α region where only the RS solution for branch 3 exists. However, in the region where the 1RSB solution appears, the simulation results seem to be trapped in the metastable 1RSB solutions. The reason for this is believed to be that the temperature $T = T_0$ is too low to realize the thermodynamic transition in the present annealing schedule. In fact, we observed the thermodynamic transition by simulations in the region where the transition

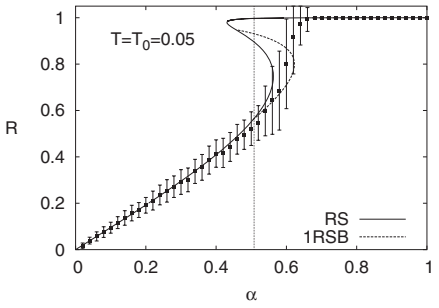

Fig. 13. α dependence of R. Solid curve: RS solution, dashed curve: 1RSB solution, $*$: simulation results with error bars. $N = 400$ and number of samples is equal to 100, $T = T_0 = 0.05$.

temperature is high. For example, when $T_0 = 0.05$ is fixed, the thermodynamic transition is observed at $T \geq 0.2$. To observe the thermodynamic transition when the transition temperature is low, we have to set an appropriate annealing schedule. We also noted in Fig. 13 that the numerical errors of the simulation results are large in the region where the 1RSB solution appears. To determine why, we calculated the histogram of overlap R for each sample. As is seen from Fig. 14, at $\alpha = 0.6$, for the majority of samples R is nearly equal to 1, and branch 3 is realized. On the other hand, for $\alpha = 0.55$ and 0.57, there are mainly two groups of samples, for one of which R is nearly equal to 1 and for the other of which R ranges from 0.4 to 0.8. It is considered that samples with $R \sim 1$ realize the RS solution for branch 3, and samples with $R = 0.4-0.8$ realize the metastable 1RSB solution and other metastable solutions. We think this is the reason for large errors of R in the simulation.

6. Summary and Discussion

We investigated the problem of the performance evaluation of the DS-CDMA multiuser detector model in low temperature regions using the replica method. We also compared theoretical results with results of Monte-Carlo simulations.

This model has three parameters: temperature T_0 that corresponds to the variance of the Gaussian channel noise, estimated temperature T, and ratio α of the number of chips of spreading codes to the number of users.

As for the stability of RS solutions, we found two types of the breaking of the replica symmetry. One is due to AT-instability (case 1), and the other is due to freezing (case 2).

The coexistence of RS solutions is possible for $T \leq 0.1$. The behavior of the solutions is different depending on whether RS solutions coexist. In the following, we describe the behavior of the solutions in each case.

When there is no region of coexistence of RS solutions in (α, T) space with T_0 fixed, both cases 1 and 2 can occur. In both cases, the value of R for the 1RSB solution is larger than the RS solution, but the difference is so small that it is indistinguishable by simulations. Therefore, we conclude that the performance of the 1RSB solution is nearly equal to the RS solution.

When a region of coexistence of RS solutions exists in (α, T) with T_0 fixed, the behavior of the solutions becomes complicated. Also, in this region, both cases 1 and 2 can take place. This region is divided into two more regions: where RS solutions bifurcate and where they do not.

First, we summarize and discuss the results on AT-stability, entropies, and free energies of RS solutions at Nishimori temperatures $T = 0.01$, 0.03, and 0.05 that we investigated. We found a sigmoidal-shaped solution that satisfies $R = q$, as in Fig. 1, when we look at the α dependence of R. It is necessary to identify a solution which is AT-stable, and has non-negative entropy and the minimum free energy. We found that solutions that are AT-stable and have positive entropies are branch 3 of the sigmoidal solution and branch 1 of the sigmoidal solution for $\alpha < \alpha_s$. Branch 2 turned out to be AT-unstable. Furthermore, a closed curve solution exists with $R \neq q$ that is AT-unstable, too. On the other hand, the free energy of branch 1 is less than branch 3 for $\alpha < \alpha_{th}$ and vice verse for $\alpha > \alpha_{th}$. Comparing α_{th} with α_s, we found that $\alpha_{th} < \alpha_s$, although these values are very close. Therefore, solutions which have the minimum free energy are branch 1 for $\alpha < \alpha_{th}$ and branch 3 for $\alpha > \alpha_{th}$. As for the 1RSB solution emerging from branch 1 at $\alpha = \alpha_s$ due to freezing, its free energy is identical to branch 1. Thus, the 1RSB solution is metastable. Therefore, we found that the breaking of replica symmetry for a metastable RS solution that takes place at Nishimori temperature does not contradict a well-known result by Nishimori in which replica symmetry for the dominant solution does not break at Nishimori temperature.[16)]

On the other hand, for other temperatures than Nishimori temperatures, a 1RSB solution with the minimum free energy due to freezing might appear when RS solutions coexist. An example is shown in Fig. 15. As well as in Nishimori temperature, in this case, when we look at the α dependence of R, a distorted sigmoidal solution and a closed

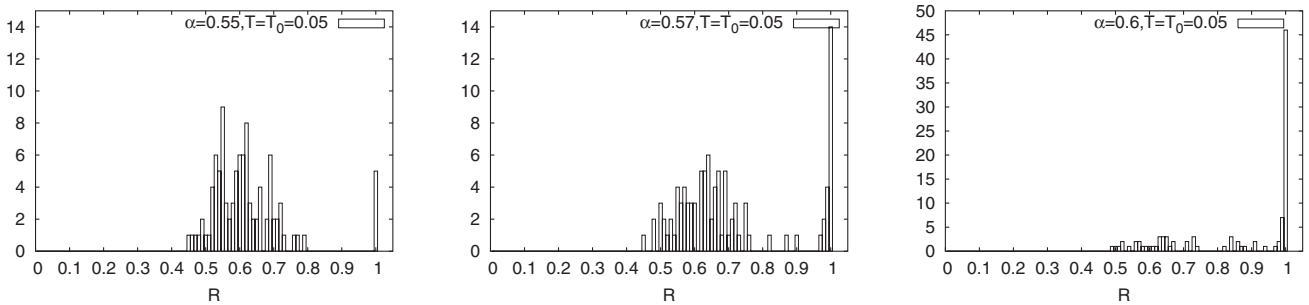

Fig. 14. Histogram of overlap R at $T = T_0 = 0.05$. $N = 400$ and number of samples is equal to 100. Left panel: $\alpha = 0.55$. Center panel: $\alpha = 0.57$. Right panel: $\alpha = 0.6$.

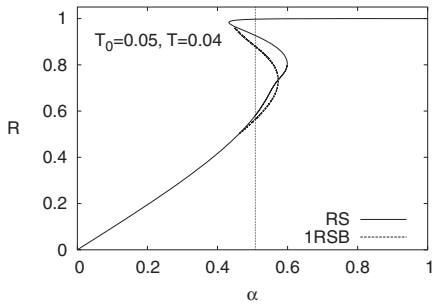

Fig. 15. α dependence of R at $T_0 = 0.05$ and $T = 0.04$. Solid curve: RS solution, dotted curve: 1RSB solution. Vertical dotted line indicates value α_{th}.

curve solution exist, and α_s and α_{th} are defined. We found that $\alpha_s < \alpha_{th}$ holds. Thus the 1RSB solution due to freezing has minimum free energy for $\alpha_s < \alpha < \alpha_{th}$. At $T_0 = 0.05$ and $T = 0.04$, we found $\alpha_s = 0.46$ and $\alpha_{th} = 0.5$. In this α region, the value of R for the 1RSB solution due to freezing is smaller than that for the RS solution for branch 1, but the difference of R is very small. Therefore, we conclude that the performance of the 1RSB solution is nearly equal to the RS solution for branch 1 for $\alpha_s < \alpha < \alpha_{th}$. We also found that case 1 occur at $T \neq T_0$; that is, the branch 3 solution becomes AT-unstable, and a 1RSB solution appears. However, its free energy is less than branch 1, and this 1RSB solution is also metastable.

Next, we discuss the bifurcation of RS solutions. The region where bifurcation takes place is located at low T_0 and T near or lower than the Nishimori temperature. When the sigmoidal curve overlaps with the closed curve with $R \neq q$ at Nishimori temperature, if T is slightly changed from T_0 with T_0 fixed, recombination between the sigmoidal and closed curves takes place. As a result, new distorted sigmoidal and new closed curve solutions appear. Since RS solutions with $R = q$ cannot exist for $T \neq T_0$, this is symmetry-breaking bifurcation with respect to symmetry $R = q$, and $R \neq q$ holds for new solutions.

We performed Monte-Carlo simulations by adopting various annealing schedules and confirmed that the simulation results agree with theoretical ones, except where RS solutions coexist and thermodynamic transition temperature is as low as $T = 0.05$. In this case, simulation results are trapped in metastable states frequently. To observe the thermodynamic transition in simulations, appropriate annealing schedules must be adopted.

Finally, we mention future problems. In the region where RS solutions coexist, comprehensive studies on the bifurcation of RS solutions and solutions which are AT-stable and have non-negative entropy and the minimum free energy are necessary. As for the stability of the freezing 1RSB solutions, since the relative relation between transition point α_{th} and α_s depends on T_0 and T, it is necessary to determine boundary $\alpha_{th} = \alpha_s$. In particular, relation $\alpha_{th} > \alpha_s$ was observed at Nishimori temperatures $T = 0.01$, 0.03, and 0.05 in this paper. However, since α_{th} and α_s were obtained numerically and are very close, the result is not definitive, and the relation must be confirmed. Furthermore, we will address the problems of AT-stability and the definition and evaluation of bit-error rate for 1RSB solutions.

1) T. Tanaka: IEEE Trans. Inf. Theory **48** (2002) 2888.
2) D. Guo and S. Verdú: IEEE Trans. Inf. Theory **51** (2005) 1983.
3) T. Tanaka: *Lecture Notes in Computer Science* (Springer, Heidelberg, 2004) Vol. 3244, p. 464.
4) A. L. Moustakas, S. H. Simon, and A. M. Sengupta: IEEE Trans. Inf. Theory **49** (2003) 2545.
5) R. Müller: IEEE Trans. Signal Process. **51** (2003) 2821.
6) C.-K. Wen and K.-K. Wong: Proc. IEEE Int. Symp. Information Theory, 2004, p. 282.
7) K. Nokura: J. Phys. A **31** (1998) 7447.
8) H. S. Seung, H. Sompolinsky, and N. Tishby: Phys. Rev. A **45** (1992) 6056.
9) T. Uezu, M. Yoshida, T. Tanaka, and M. Okada: Prog. Theor. Phys. Suppl. No. 157 (2005) 254.
10) S. Verdú: *Multiuser Detection* (Cambridge University Press, Cambridge, 1988).
11) H. Nishimori: *Statistical Physics of Spin Glasses and Information Processing: An Introduction* (Oxford University Press, Oxford, 2001).
12) N. Sourlas: Nature **339** (1989) 693.
13) Y. Kabashima and D. Saad: Europhys. Lett. **45** (1999) 97.
14) J. R. L. de Almeida and D. J. Thouless: J. Phys. A **11** (1978) 983.
15) W. Krauth and M. Mézard: J. Phys. (Paris) **50** (1989) 3057.
16) H. Nishimori: Europhys. Lett. **57** (2002) 302.